Optik - International Journal for Light and Electron Optics 288 (2023) 171247

Contents lists available at ScienceDirect

Optik

journal homepage: www.elsevier.com/locate/ijleo

High-performance terahertz polarization filter based on the anti-resonant fiber

Qiang Liu [a], Guangrong Sun [a], Yudan Sun [b], Tongyu Meng [c], Haiwei Mu [a], Wei Liu [a], Chao Ma [a], Wenjing Li [a], Kaiyu Wang [a], Jingwei Lv [a], Paul K. Chu [d], Chao Liu [a,*]

[a] School of Physics and Electronic Engineering, Northeast Petroleum University, Daqing 163318, China
[b] College of Mechanical and Electrical Engineering, Daqing Normal University, Daqing 163712, China
[c] Leicester International Institute, Dalian University of Technology, Dalian 124221, China
[d] Department of Physics, Department of Materials Science and Engineering, and Department of Biomedical Engineering, City University of Hong Kong, Tat Chee Avenue, Kowloon, Hong Kong, China

ARTICLE INFO

Keywords:
Anti-resonant fiber
Polarization filter
Terahertz
High-resistivity silicon

ABSTRACT

A novel terahertz polarization filter based on the anti-resonant fiber is designed and analyzed. The polarization extinction ratio (PER) is improved by using high-resistivity silicon (HRS) as the bulk material in conjunction with a double conjoined tube cladding structure. The effects of the structure and material of the anti-resonant fiber on the polarization filtering characteristics are analyzed by the finite element method. The PER of the anti-resonant fiber reaches 100 dB and the insertion loss of y-polarization fundamental mode (YPFM) is less than 0.66 dB at 1 THz when the anti-resonant fiber length is 5.58 cm. The bandwidth can be expanded by changing the fiber length and for a fiber length of 8 cm, the frequency bandwidth is 0.92–1.14 THz and the insertion loss is less than 3 dB. The polarization filter is demonstrated to deliver excellent performance in the terahertz frequency range and has large commercial potential in terahertz communication and biomedical spectroscopy.

1. Introduction

Terahertz waves have great potential in non-destructive imaging [1], medical examination [2], security surveillance [3], terahertz communication [4], sensing [5], drug detection [6], and military applications [7]. In order to construct a compact structure for remote transmission of terahertz waves, several kinds of dielectric waveguides composed of metallic wires [8], dielectric tubes with metal coatings [9], sub-wavelength fibers [10], porous fibers [11], photonic bandgap fibers [12], and anti-resonant fibers [13] have been proposed. In particular, anti-resonant fibers have received extensive attention due to their outstanding transmission characteristics such as small nonlinearity, low transmission loss, negligible dispersion, as well as large bandwidth [14,15].

In terahertz communication, terahertz polarization filters can reduce channel scattering and multipath interference during data transmission, improve signal quality and reliability [16]. In addition, terahertz also has potential in biomedical spectroscopy. The terahertz polarization filters can improve the light coupling efficiency, reduce light intensity loss and image distortion, thus improving diagnostic accuracy and therapeutic effect [17]. The high-performance polarization filters require that one of the two orthogonal polarization fundamental modes can be transmitted with low loss, while the other modes are suppressed. Y. Hou et al. [18] have

* Corresponding author.
E-mail address: msm-liu@126.com (C. Liu).

https://doi.org/10.1016/j.ijleo.2023.171247
Received 31 March 2023; Received in revised form 29 June 2023; Accepted 30 July 2023
Available online 1 August 2023

reported a terahertz polarization filter based on the hollow core fiber with PTFE showing a loss difference of only 0.036 dB/cm at 1.675 THz and polarization extinction ratio (PER) of 30 dB for a fiber length of 8.33 m. S. Zhou et al. [19] have adopted the terahertz sub-wavelength fiber in designing a polarization filter composed of Topas and PET. The PER is 30 dB within a dozen centimeters and the insertion loss of the fundamental mode is less than 4 dB. A. Mollah et al. [14] have proposed a terahertz anti-resonant fiber for the polarization filter using Zeonex and the PER is 10 dB at 1 THz. X. Jiang et al. [15] have numerically analyzed a terahertz anti-resonant fiber comprising two circular tubes based on Topas. The PER reaches 30 dB for a fiber length of 7.44 cm and the insertion loss is less than 2.7 dB at 1 THz. It has been observed that the choice of materials is crucial to the polarization filter design. In the terahertz range, the common dielectric waveguide materials include Topas [20], Zeonex [21], PMMA [22], Teflon [23], PTFE [24], PET [25], and HRS [26]. The material absorption coefficient of HRS is less than 0.015 cm^{-1} in the range of 0.1–1.5 THz thus producing low effective material loss. Meanwhile, the refractive index change is only 0.0001 in the range of 0.5–4.5 THz, and it can essentially be regarded as having no dispersion [26].

Herein, a polarization filter based on the anti-resonant fiber with HRS is designed for the terahertz frequency range, and the effects of the structure and material of the anti-resonant fiber on the polarization filtering properties are analyzed. The results show that a PER of 100 dB can be achieved when the fiber length is 5.58 cm, and the insertion loss of YPFM is less than 0.66 dB at 1 THz. Compared to the previously reported terahertz polarization filter based on the anti-resonant fiber, our proposed structure consisting of a semi-circular lattice tube and semi-elliptical lattice tube provides rich design dimension for multi-parameter optimization and effectively improves the performance of terahertz polarization filters.

2. Modeling and analysis

The anti-resonant fiber is depicted schematically in Fig. 1. The white area represents air and the cladding consists of two conjoined lattice tubes with a spacing d of 0.09 mm fixed on the inner wall of the jacket tube. Each conjoined tube is formed by splicing a semi-circular lattice tube and semi-elliptical lattice tube. The semi-major axis and semi-minor axis of the outer wall of the semi-elliptical tubes are r_a and r_b, respectively. The inner radius of the jacket tube is $R = 0.74$ mm. The relationship between R, d, r_a, and r_b is $r_a = R\text{-}d/2\text{-}r_b$, and the wall thickness of the cladding tubes is $t = 0.022$ mm. The thickness of the jacket tube is $JT = 0.1$ mm, and the thickness of the perfectly matched layer is $T = 0.2$ mm. The possible manufacturing methods of terahertz anti-resonant fiber include stacking [27], extrusion [28] and 3D printing [29]. The stacking method is feasible for the compact cladding tubes structure. The proposed anti-resonant fiber has only two cladding tubes that are not well fixed and is not suitable for stacking method. The extrusion method is easily to deform the cladding tubes. It is believed that 3D printing method can be used to fabricate our proposed anti-resonant fiber in the future. The finite element method (FEM) is used to analyze and optimize the anti-resonant fiber. In order to improve the simulation accuracy, an extremely fine mesh size of $\lambda/10$ is used in the HRS.The choice of such mesh size provide excellent agreement with the Ref [15]. The refractive index of HRS material is set to be a constant of 3.417 in the range of 0.5–4.5 THz due to the small refractive index changing rate [26].

According to the principle of the hollow core anti-resonant fiber (HC-ARF), the working bandwidth should avoid the resonant frequency. Therefore, it is necessary to compute the resonant frequency by Eq. (1) [30,31]:

$$f_c = \frac{mc}{2t\sqrt{n^2 - 1}} \tag{1}$$

where c is the speed of light in free space, m is the resonant order, n is the refractive index of HRS material, t is the wall thickness of the cladding tubes. For $n = 3.417$, $m = 1$, and $t = 0.022$ mm, the corresponding resonant frequency f_c is 2.08 THz which is away from 1 THz.

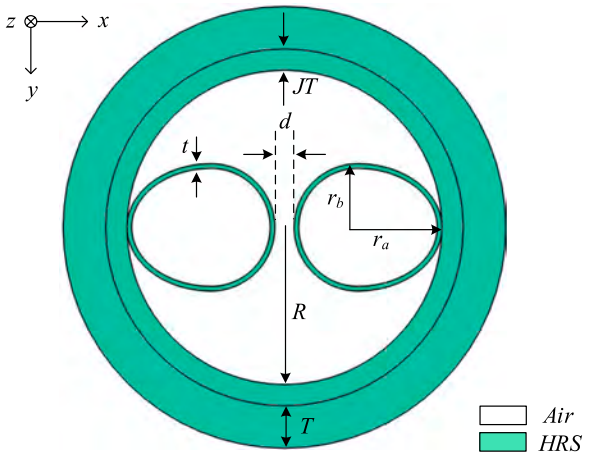

Fig. 1. Cross-section of the anti-resonant fiber.

The filtering characteristics of the polarization filter can be determined using the polarization extinction ratio (PER) as shown in Eq. (2) [32,33]:

$$PER = 10\log_{10}\frac{P_{out}(M1)}{P_{out}(M2)} \tag{2}$$

where $P_{out}(M1)$ and $P_{out}(M2)$ represent the output power of mode 1 and mode 2 with equal incident power, which can be calculated by Eq. (3) [32,33]:

$$P_{out} = \exp(-TL \times L \times \frac{\ln 10}{10}) \tag{3}$$

where TL is the total loss of a certain mode and L is the fiber length. At the same time, $TL \times L$ is known as the insertion loss (IL) of the polarization filter.

The transmission loss of the anti-resonant fiber includes mainly the confinement loss (CL) and effective material loss (EML). The confinement loss describes the optical field leakage of the anti-resonant fiber and is determined by the fiber structure and unavoidable in theory. The confinement loss can be calculated by Eq. (4) [34,35]:

$$CL = 8.686\left(\frac{2\pi f}{c}\right)Im(n_{eff}) \times 10^{-2}, [dB/cm] \tag{4}$$

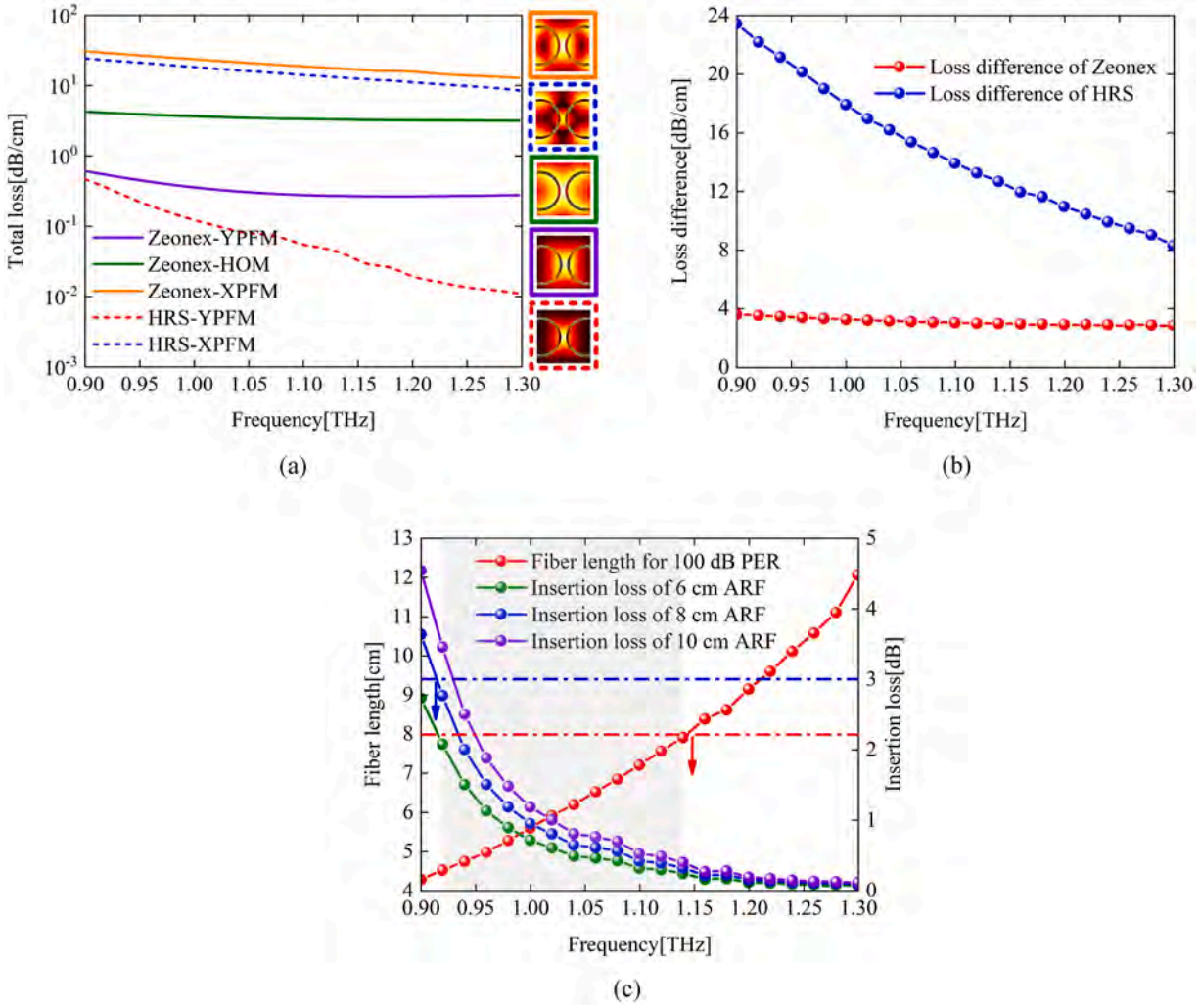

Fig. 2. Transmission characteristics of the anti-resonant fiber made of different materials: (a) Total loss of different modes for Zeonex and HRS, (b) Loss difference between the minimum unwanted mode and wanted mode for Zeonex and HRS and (c) Required fiber length for 100 dB PER and insertion losses of different fiber lengths.

where f is the operating frequency and $Im(n_{eff})$ is the imaginary part of the effective refractive index. The effective material loss refers to the inherent absorption loss of the fiber expressed by Eq. (5) [30,31]:

$$EML = 4.34\sqrt{\frac{\varepsilon_0}{\mu_0}}\frac{\int_{A_{mat}} n\alpha_{mat}|E|^2 dA}{2\int_{All} S_z dA}, [dB/cm] \tag{5}$$

where ε_0 and μ_0 are the permittivity and permeability in free space, respectively, α_{mat} is the material absorption coefficient of HRS and S_z is the z-component of the Poynting vector, which can be expressed as $S_z = \frac{1}{2}\mathrm{Re}(E \times H^*)z$, where E is the electric field and H is the magnetic field.

2.1. Comparison of different materials

The effect of the material on the polarization filter is analyzed and compared. For $JT = 0.1$ mm, $t = 0.022$ mm, $d = 0.09$ mm, $r_b = 0.3$ mm and $R = 0.74$ mm, the loss spectra of different modes are shown in Fig. 2(a). As for Zeonex, the anti-resonant fiber can support YPFM, XPFM, and higher order mode (HOM) transmission in the range of 0.9–1.3 THz. The electric field diagrams of the three modes at 1 THz are shown in the insets of Fig. 2(a). YPFM is well confined in the core region and the electric fields of XPFM and HOM leak partially into the cladding region. Therefore, the total loss of YPFM is the lowest, whereas XPFM and HOM have higher losses. With regard to HRS, the anti-resonant fiber only supports YPFM and XPFM transmission in the core region. YPFM is confined better in the core region by comparing the electric field diagrams of YPFM and XPFM.

According to Eq. (2), the extinction ratio of the polarization filter depends on the loss difference between the minimum unwanted mode and wanted mode. The loss differences for Zeonex and HRS are presented in Fig. 2(b). Compared to Zeonex, HRS has a greater loss difference and better polarization extinction performance.

Eq. (2) and Eq. (3) show that the extinction ratio of the polarization filter is determined by the length of the anti-resonant fiber. Fig. 2(c) presents the required fiber length for different frequencies as the PER reaches 100 dB. The required fiber length increases with frequencies and the anti-resonant fiber shows a greater loss difference at low frequencies. In the range of 0.9–1.3 THz, the fiber length is changed from 4.26 to 12.06 cm. It means that the anti-resonant fiber can achieve an extinction ratio of 100 dB with a shorter fiber and the fiber length is 5.58 cm at 1 THz. In the actual polarization filter, the fiber length is fixed. In order to achieve simultaneous 100 dB PER, wider working bandwidth, and lower insertion loss, Fig. 2(c) exhibits the insertion losses for fiber lengths of 6 cm, 8 cm, and 10 cm. The effect of the fiber length on the insertion loss is not substantial but impacts the working bandwidth. Here, the fiber length can be tailored to meet the requirement of the operating frequency and insertion loss. For instance, for a fiber length of 8 cm, the insertion loss is less than 3 dB and PER is 100 dB in the range of 0.92–1.14 THz.

2.2. Optimization of the gap spacing d

For $JT = 0.1$ mm, $t = 0.022$ mm, $r_b = 0.3$ mm and $R = 0.74$ mm, the effect of the gap spacing d on the loss at 1 THz is shown in Fig. 3(a). The effective material loss of YPFM and XPFM is very small, and so the total loss is mainly contributed by the confinement loss. With increasing d, the total loss of YPFM decreases first and then increases gradually, while the total loss of XPFM increases slowly. The total loss of XPFM is bigger than the total loss of YPFM due to stronger coupling between XPFM and cladding modes with increasing d [36]. Fig. 3(b) shows the polarization extinction ratio and insertion loss when the fiber length is 5.58 cm. The PER

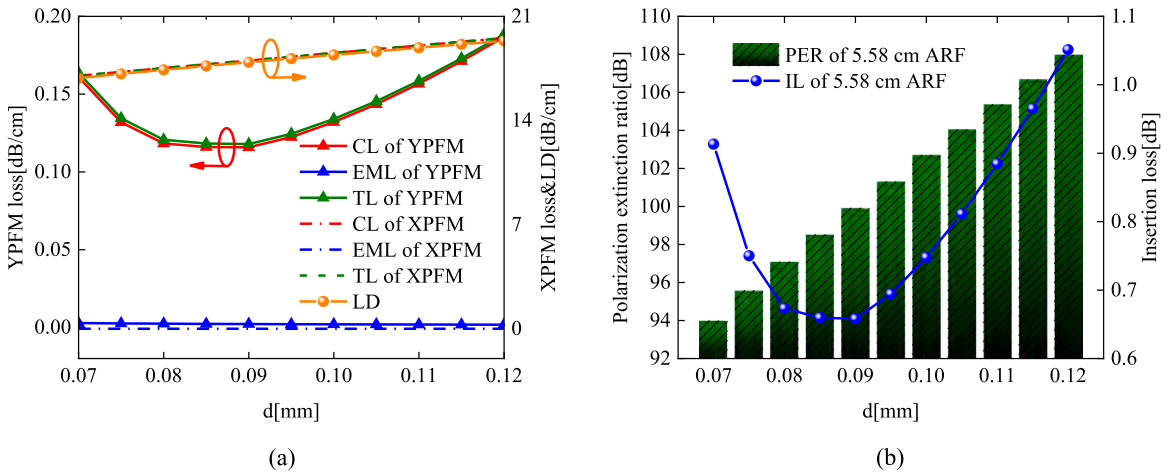

Fig. 3. Effect of the gap spacing d on loss, PER, and IL: (a) Confinement loss, effective material loss, total loss of XPFM and YPFM, and loss difference between XPFM and YPFM and (b) PER and IL for a fiber length of 5.58 cm.

increases with d and meanwhile, the IL decreases initially and then increases. In order to obtain a larger polarization extinction ratio and smaller insertion loss at the same time, $d = 0.09$ mm is selected as the optimal value.

2.3. Optimization of the outer semi-minor axis r_b

For $JT = 0.1$ mm, $t = 0.022$ mm, $d = 0.09$ mm and $R = 0.74$ mm, the effect of the outer semi-minor axis r_b on the loss at 1 THz is displayed in Fig. 4(a). With increasing r_b, the total loss of YPFM increases initially and then decreases, and the maximum appears near $r_b = 0.23$ mm. It is because the outer semi-minor axis affects the effective refractive index of YPFM. As it approaches the effective refractive index of the cladding mode, mode coupling becomes stronger [37,38]. The total loss of XPFM increases monotonically and is greater than that of YPFM. The loss difference between the XPFM and YPFM is mainly determined by XPFM, as shown by the orange dotted line in Fig. 4(a). The polarization extinction ratio exhibits the same trend with increasing r_b as shown in Fig. 4(b). The insertion loss is lower as r_b is changed from 0.29 mm to 0.34 mm. In order to obtain a better polarization extinction performance and lower insertion loss, $r_b = 0.3$ mm is chosen as the optimal value.

2.4. Optimization of the fiber inner radius R

The effect of the fiber inner radius R on the properties of the polarization fiber is investigated. For $JT = 0.1$ mm, $t = 0.022$ mm, $d = 0.09$ mm and $r_b = 0.3$ mm, the loss at 1 THz for different fiber inner radii are shown in Fig. 5(a). The total losses of YPFM and XPFM depend on the confinement losses and decrease monotonically with increasing R. The loss difference almost overlaps the total loss of XPFM due to the larger difference between the two polarization fundamental modes. Fig. 5(b) shows the polarization extinction ratio and insertion loss when the fiber length is 5.58 cm. The polarization extinction ratio decreases with R, while the insertion loss varies in a small range and can be neglected. In order to accomplish a polarization extinction ratio of 100 dB, $R = 0.74$ mm is selected.

Based on the above analysis, the optimized parameters of our proposed terahertz polarization filter based on the anti-resonant fiber are set as $d = 0.09$ mm, $r_b = 0.3$ mm and $R = 0.74$ mm. Therefore, we can achieve a PER of 100 dB and the insertion loss of YPFM is less than 0.66 dB at 1 THz when the anti-resonant fiber length is 5.58 cm. As demonstrated in Table 1, the polarization filtering properties of our proposed fiber exhibit better performance compared with other existing terahertz fibers.

3. Fabrication tolerance

In terahertz communication, fabrication tolerance can affect the performance of terahertz polarization filters and then influence the quality and stability of communication system. In addition, the design and tolerance of terahertz polarization filters may influence biomedical spectroscopy including imaging resolution and depth, as well as the ability to detect specific tissues and organs. Therefore, it is necessary to investigate the effect of fabrication tolerance on the properties of our proposed terahertz polarization filter. Fig. 6(a) shows the total loss of YPFM and XPFM if the left tube deviates by 10°. The asymmetrical structure has little impact on the loss of YPFM and XPFM compared to the standard structure and so the difference is negligible. Meanwhile, the wall thickness of the two tubes may be different. Fig. 6(b) shows the total loss of YPFM and XPFM when the wall thicknesses of the right and left cladding tubes are $t_0 = 0.0215$ mm and $t = 0.022$ mm respectively. Compared to the perfectly symmetrical structure, the deviation in the wall thickness has little impact on the loss of YPFM and only slightly affects the loss of XPFM at higher frequencies, but the influence is not substantial. Our analysis reveals that minor structural deviations have little effect on the performance of the polarization filter with robust transmission characteristics.

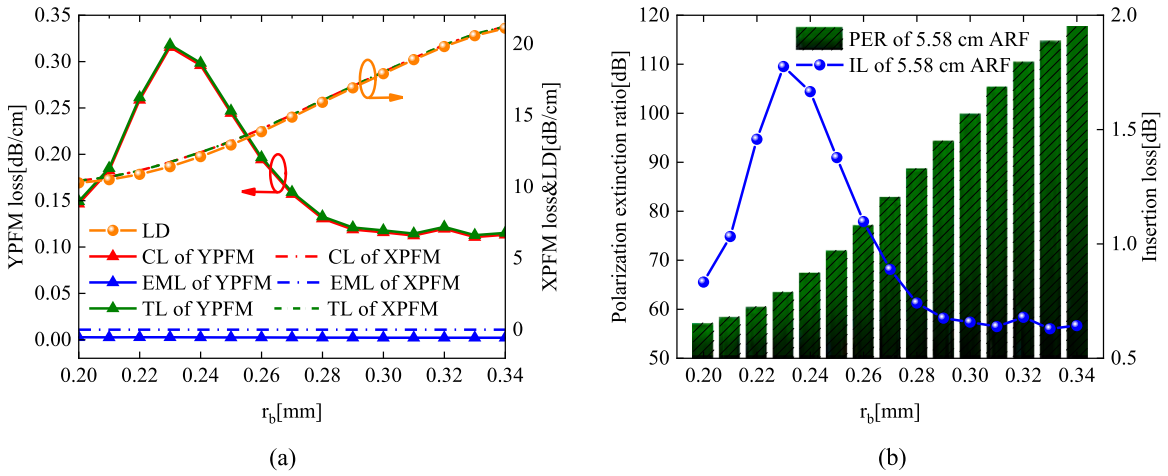

Fig. 4. Effect of the outer semi-minor axis r_b on loss, PER, and IL: (a) Confinement loss, effective material loss, total loss of XPFM and YPFM, and loss difference between XPFM and YPFM and (b) PER and IL for a fiber length of 5.58 cm.

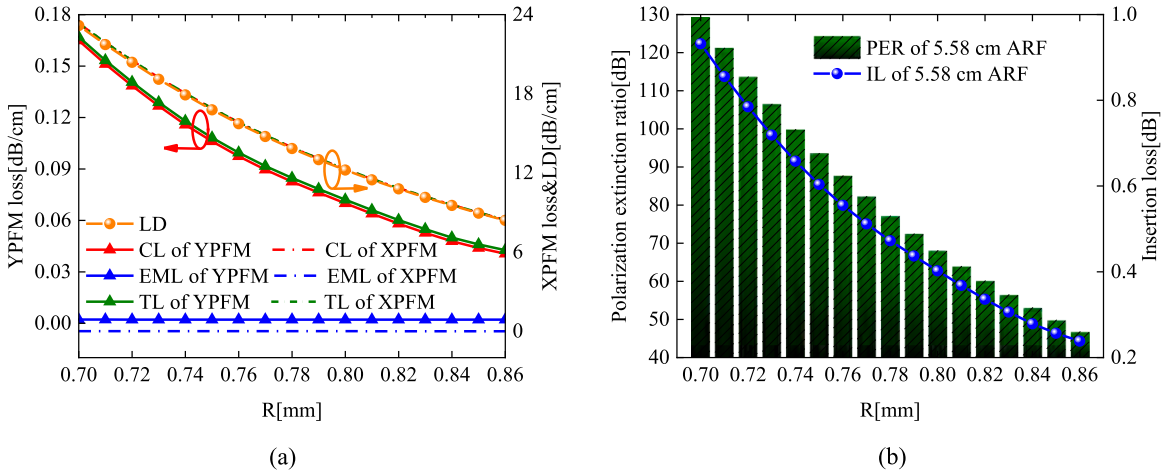

Fig. 5. Effect of the fiber inner radius R on loss, PER, and IL: (a) Confinement loss, effective material loss, total loss of XPFM and YPFM, and loss difference between XPFM and YPFM and (b) PER and IL for a fiber length of 5.58 cm.

Table 1
Comparison between our proposed fiber and other existing terahertz fibers.

Reference	Fiber type	Material type	LD (dB/cm)	PER (dB)	Operating frequency (THz)
Ref. [18]	HCF	PTFE	0.036	30@8.33 m	1.675
Ref. [19]	SWF	Topas & PET	/	30@6.01–15.44 cm	/
Ref. [14]	ARF	Zeonex	/	~10	1.0
Ref. [15]	ARF	Topas	4.03	30@7.44 cm	1.0
This work	ARF	HRS	17.91	100@5.58 cm	1.0

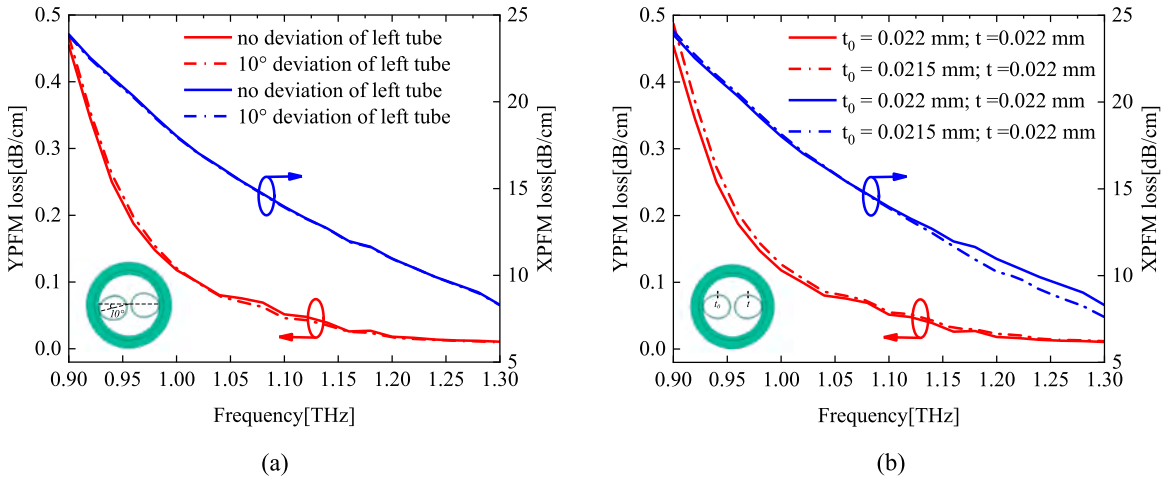

Fig. 6. (a) Transmission characteristics of the anti-resonant fiber when the left tube has a 10° deviation with respect to the fiber center and (b) Transmission characteristics of the anti-resonant fiber when the left tube has a different wall thickness t_0.

4. Conclusion

A polarization filter based on the terahertz anti-resonant fiber with high PER is designed and analyzed. HRS is used as the bulk material to decrease the effective material loss of the anti-resonant fiber and improve its properties. At 1 THz, the PER is 100 dB, the corresponding fiber length is 5.58 cm, and the insertion loss of YPFM is less than 0.66 dB. In addition, the working bandwidth can be expanded by increasing the fiber length. The polarization filter with excellent characteristics has large potential in terahertz applications.

Declaration of Competing Interest

The manuscript has not been previously published, is not currently submitted for review to any other journal, and will not be submitted elsewhere before a decision is made by this journal. The authors declare no conflicts of interest.

Data availability

The data that has been used is confidential.

Acknowledgements

This work was jointly supported by the Hainan Province Science and Technology Special Fund [ZDYF2022GXJS003], Local Universities Reformation and Development Personnel Training Supporting Project from Central Authorities, Natural Science Foundation of Heilongjiang Province [grant number LH2021F007], China Postdoctoral Science Foundation funded project [grant number 2020M670881], City University of Hong Kong Strategic Research Grant (SRG) [grant number 7005505], and City University of Hong Kong Donation Research Grant [grant number DON-RMG 9229021].

References

[1] K. Kawase, Y. Ogawa, Y. Watanabe, Non-destructive terahertz imaging of illicit drugs using spectral fingerprints, Opt. Express 11 (20) (2003) 2549–2554.
[2] C.J. Strachan, P.F. Taday, D.A. Newnham, Using terahertz pulsed spectroscopy to quantify pharmaceutical polymorphism and crystallinity, J. Pharm. Sci. 94 (4) (2005) 837–846.
[3] N. Laman, S.S. Harsha, D. Grischkowsky, 7 GHz resolution waveguide THz spectroscopy of explosives related solids showing new features, Opt. Express 16 (6) (2008) 4094–4105.
[4] A. Barh, B.P. Pal, G.P. Agrawal, Specialty fibers for terahertz generation and transmission: a review, IEEE J. Sel. Top. Quant. 22 (2) (2016), 8500215.
[5] D. Abbott, X. Zhang, Scanning the Issue: T-Ray imaging, sensing, and retection, Proc. IEEE 95 (8) (2007) 1509–1513.
[6] M. Nagel, P.H. Bolivar, M. Brucherseifer, Integrated THz technology for label-free genetic diagnostics, Appl. Phys. Lett. 80 (1) (2002) 154–156.
[7] D.J. Cook, B.K. Decker, M.G. Allen, Quantitative THz spectroscopy of explosive materials, Opt. Terahertz Sci. Technol. (2005).
[8] K. Wang, D.M. Mittleman, Metal wires for terahertz wave guiding, Nature 432 (2004) 376–379.
[9] B. Bowden, J.A. Harrington, O. Mitrofanov, Fabrication of terahertz hollow-glass metallic waveguides with inner dielectric coatings, J. Appl. Phys. 104 (9) (2008), 093110.
[10] J.Y. Lu, C.M. Chiu, C.C. Kuo, Terahertz scanning imaging with a subwavelength plastic fiber, Appl. Phys. Lett. 92 (8) (2008), 084102.
[11] A. Hassani, A. Dupuis, M. Skorobogatiy, Low loss porous terahertz fibers containing multiple subwavelength holes, Appl. Phys. Lett. 92 (7) (2008), 071101.
[12] L. Vincetti, Hollow core photonic band gap fiber for THz applications, Microw. Opt. Technol. Lett. 51 (7) (2009) 1711–1714.
[13] F. Poletti, Nested antiresonant nodeless hollow core fiber, Opt. Express 22 (20) (2014) 23807–23828.
[14] A. Mollah, S. Rana, H. Subbaraman, Polarization filter realization using low-loss hollow-core anti-resonant fiber in THz regime, Results Phys. 17 (2020), 103092.
[15] X. Jiang, H. Yang, W. Luo, Twin-tube terahertz fiber for a polarization filter, Opt. Express 30 (18) (2022) 31806–31815.
[16] I.F. Akyildiz, J.M. Jornet, C. Han, Terahertz band: next frontier for wireless communications, Phys. Commun. 12 (2014) 16–32.
[17] A. Gong, Y. Qiu, X. Chen, Biomedical applications of terahertz technology, Appl. Spectrosc. Rev. 55 (5) (2019) 418–438.
[18] Y. Hou, F. Fan, H. Zhang, Terahertz single-polarization single-mode hollow-core fiber based on index-matching coupling, IEEE Photonics Technol. Lett. 24 (8) (2012) 637–639.
[19] S. Zhou, H. Chan, L. Reekie, Polymer fiber polarizer for terahertz applications, IEEE Photonics Technol. Lett. 24 (17) (2012) 1490–1492.
[20] M. Meng, D. Yan, Z. Yuan, Novel double negative curvature elliptical aperture core fiber for terahertz wave transmission, J. Phys. D Appl. Phys. 54 (2021), 235102.
[21] S. Hossain, A. Mollah, K. Hosain, THz spectroscopic sensing of liquid chemicals using hollow-core anti-resonant fiber, OSA Continuum. 4 (2) (2021) 621–632.
[22] D. Yan, J. Li, Design and analysis of the influence of cladding tubes on novel THz waveguide, Optik 180 (2019) 824–831.
[23] V. Kumar, R.K. Varshney, S. Kumar, Terahertz generation by four-wave mixing and guidance in diatomic teflon photonic crystal fibers, Opt. Commun. 454 (2020), 124460.
[24] A. Elakkiya, S. Radha, B.S. Sreeja, Terahertz broadband metamaterial absorber enabled by SiO_2, polyimide and PET dielectric substrates, Pramana J. Phys. 94 (2020) 130.
[25] Y.S. Lee, H. Choi, B. Kim, Low-loss polytetrafluoroethylene hexagonal porous fiber for terahertz pulse transmission in the 6G mobile communication window, IEEE Trans. Microw. Theory Tech. 69 (11) (2021) 4623–4630.
[26] J. Dai, J. Zhang, W. Zhang, Terahertz time-domain spectroscopy characterization of the far-infrared absorption and index of refraction of high-resistivity, float-zone silicon, J. Opt. Soc. Am. B 21 (7) (2004) 1379–1386.
[27] V. Setti, L. Vincetti, A. Argyros, Flexible tube lattice fibers for terahertz applications, Opt. Express 21 (3) (2013) 3388–3399.
[28] W. Talataisong, J. Gorecki, L.D.V. Putten, Hollow-core antiresonant terahertz fiber-based TOPAS extruded from a 3D printer using a metal 3D printed nozzle, Photonics Res. 9 (8) (2021) 1513–1521.
[29] A.L.S. Cruz, C.M.B. Cordeiro, M.A.R. Franco, 3D printed hollow-core terahertz fibers, Fibers 6 (30) (2018) 6030043.
[30] A. Mollah, S. Habib, S. Habib, Novel hollow-core asymmetric conjoined-tube anti-resonant fiber for low-loss THz wave guidance, OSA Continuum 3 (5) (2020) 1169–1176.
[31] G. Sun, Q. Liu, H. Mu, Anti-resonant fiber with nested U-shape tubes for low-loss terahertz waveguides, Opt. Laser Technol. 163 (2023), 109424.
[32] L. Jiang, Y. Zheng, J. Yang, An ultra-broadband single polarization filter based on plasmonic photonic crystal fiber with a liquid crystal core, Plasmonics 12 (2017) 411–417.
[33] H. Chen, S. Li, M. Ma, Ultrabroad bandwidth polarization filter based on d-shaped photonic crystal fibers with gold film, Plasmonics 10 (2015) 1239–1242.
[34] W. Liu, Y. Shi, Z. Yi, Surface plasmon resonance chemical sensor composed of a microstructured optical fiber for the detection of an ultra-wide refractive index range and gas-liquid pollutants, Opt. Express 29 (25) (2021) 40734–40747.
[35] M. Han, Q. Liu, Y. Sun, A novel nested three-ring-core photonic crystal fiber for OAM transmission, Optik 270 (2022), 169981.
[36] C. Wei, C.R. Menyuk, J. Hu, Geometry of chalcogenide negative curvature fibers for CO_2 laser transmission, Fibers 6 (40) (2018), 6040074.
[37] F. Meng, B. Liu, Y. Li, Low loss hollow-core antiresonant fiber with nested elliptical cladding elements, IEEE Photonics J. 9 (1) (2017), 7100211.
[38] S. Sun, W. Shi, Q. Sheng, Polarization-maintaining terahertz anti-resonant fibers based on mode couplings between core and cladding, Results Phys. 25 (2021), 104309.